ZnO_{1-x} Nanorod Arrays/ZnO Thin Film Bilayer Structure: From Homojunction Diode and High-Performance Memristor to Complementary 1D1R Application

Chi-Hsin Huang,[†] Jian-Shiou Huang,[†] Shih-Ming Lin,[†] Wen-Yuan Chang,[‡] Jr-Hau He,[‡] and Yu-Lun Chueh[†,*]

[†]Department of Materials Science & Engineering, National Tsing-Hua University, Hsinchu 30013, Taiwan, Republic of China, and [‡]Department of Electrical Engineering & Institute of Photonics and Optoelectronics, National Taiwan University, Taipei 10617, Taiwan, Republic of China

ABSTRACT We present a ZnO_{1-x} nanorod array (NR)/ZnO thin film (TF) bilayer structure synthesized at a low temperature, exhibiting a uniquely rectifying characteristic as a homojunction diode and a resistive switching behavior as memory at different biases. The homojunction diode is due to asymmetric Schottky barriers at interfaces of the Pt/ZnO NRs and the ZnO TF/Pt, respectively. The ZnO_{1-x} NRs/ZnO TF bilayer structure also shows an excellent resistive switching behavior, including a reduced operation power and enhanced performances resulting from supplements of confined oxygen vacancies by the ZnO_{1-x} NRs for rupture and recovery of conducting filaments inside the ZnO TF layer. A hydrophobic behavior with a contact angle of ~125° can be found on the ZnO_{1-x} NRs/ZnO TF bilayer structure, demonstrating a self-cleaning effect. Finally, a successful demonstration of complementary 1D1R configurations can be achieved by simply connecting two identical devices back to back in series, realizing the possibility of a low-temperature all-ZnO-based memory system.

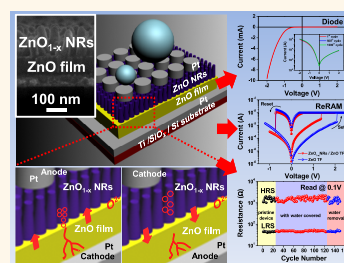

KEYWORDS: resistive switching · nonvolatile memory · ZnO_{1-x} nanorod arrays · homojunction diode · complementary 1D1R

Next-generation nonvolatile memories, such as magnetic random access memory (MRAM),[1] phase-change random access memory (PCRAM),[2] and resistive random access memory (ReRAM),[3−5] have been attracting much attention due to their significant potential for the replacement of flash memory. Among all the nonvolatile memories, the ReRAM device is the most promising candidate, which has a simple metal−insulator−metal (MIM) configuration with faster switching speed, high stacking density, lower power consumption, excellent scalability, and easier fabrication process.[3−5]

To date, two resistive switching mechanisms, namely, filamentary resistive switching and homogeneous interface resistive switching, were reported.[4] For the filamentary resistive switching, variable locations, random orientations, and uncertain sizes of conducting filaments result in a large variation of switching voltages and nonunifrom resistance states, thereby an unstable programming response.[3−5] By optimizing structural defects,[6] doping of oxide materials,[7−10] adaptation from the active bottom/top electrode materials,[11] using the bilayer structures,[12,13] and inserting metallic nanocrystals in an insulating layer,[14−16] the locations and orientations of the conducting filaments can be controlled. Nevertheless, none of these approaches based on one-dimensional nanostructure have been used to directly confine the recovery and rupture of the conducting filaments, yielding a high-performance ReRAM device. On the other hand, passive crossbar arrays *via* three-dimensional (3D) structures are being explored to geometrically achieve the maximum packing density, while sneak paths, an inherent disadvantage where a leakage current (sneak path current) can flow through the neighboring devices, are a remaining issue, leading to not only unnecessary power consumption but also a misreading problem.[17−20] To avoid sneak paths, vertical connection of a diode and a resistive memory together, namely, 1D1R, is the simplest approach to achieve 3D crossbar arrays with the highest stacking density.

In this article, we present the growth of ZnO_{1-x} nanorod arrays (NRs) on a ZnO thin film (TF) as homojunction diode and memory devices, containing uniquely double behaviors, namely, rectifying and resistive

* Address correspondence to ylchueh@mx.nthu.edu.tw.

Received for review July 19, 2012 and accepted August 18, 2012.

Published online August 18, 2012
10.1021/nn303233r

© 2012 American Chemical Society

switching behaviors, depending on the applied voltages simultaneously. The ZnO_{1-x} NRs can not only create asymmetric Schottky barriers at interfaces of the Pt/ZnO NRs and the ZnO TF/Pt, resulting in a homojuntion diode, but also provide the oxygen vacancies from the ZnO_{1-x} NRs for the recover and rupture of conducting filaments in the ZnO TF layer, thereby stabilizing operation performances. In addition, by utilizing the ZnO_{1-x} NR surface, a contact angle of ~125° can be achieved, demonstrating a self-cleaning effect due to hydrophobic behavior. Finally, we are able to successfully demonstrate a complementary 1D1R memory system by connecting two identical devices back to back in series, providing a low-temperature all-ZnO-based memory system.

RESULTS AND DISCUSSION

To fabricate the ZnO_{1-x} NRs/ZnO TF bilayer structure, a ZnO TF with a thickness of 100 nm was deposited on a Pt (100 nm)/Ti (20 nm)/SiO_2 (400 nm)/Si substrate at room temperature by a radio frequency (rf)-magnetron sputter as the resistive switching layer and seed layer for the growth of the ZnO_{1-x} NRs *via* the chemical bath deposition process at 95 °C (see Supporting Information for more details). Figure 1a shows a schematic of the ZnO_{1-x} NRs grown on the ZnO TF bilayer device, with which the Pt metal as the top electrode was deposited on the ZnO_{1-x} NRs by rf-magnetron sputter at room temperature. The ZnO thin film deposited by the sputter process has a polycrystalline structure with a weak *c*-axis orientation,[21] while the single-crystalline structure of ZnO NRs could be achieved by the chemical solution process with a distinct growth direction along the *c*-axis, namely, the [0001] direction.[22] The corresponding SEM image of one-dimensional, high-density, and well-aligned ZnO_{1-x} NRs grown on the ZnO TF with a average length of 150 nm is shown in Figure 1b. In order to identify the oxygen distribution from the ZnO_{1-x} NRs to the ZnO TF layers, XPS spectra at the O 1s-edge related to the corresponding positions from a to e in the SEM image (Figure 1b) were carried out as shown in Figure 1c. A distinct peak at ~532 eV owing to the nonlattice oxygen bonding indicates the presence of unbonded oxygen molecules (oxygen interstitials) and oxygen vacancies located in the ZnO_{1-x} NRs, while a peak at ~530 eV related to the lattice oxygen bonding reveals a few oxygen vacancies and structural defects in the ZnO TF layer.[23]

Notably, the different densities of oxygen vacancies distributed in the ZnO_{1-x} NRs and ZnO TF result in an asymmetric Schottky barrier height, leading to a rectifying characteristic as shown in Figure 2a, while the Pt/ZnO/Pt device without the growth of the ZnO_{1-x} NRs shows the symmetric $I-V$ characteristic (Supporting Figure S1). The inset shows the corresponding current density at different voltages, with which a turn-on voltage of −0.6 V and a forward current density of

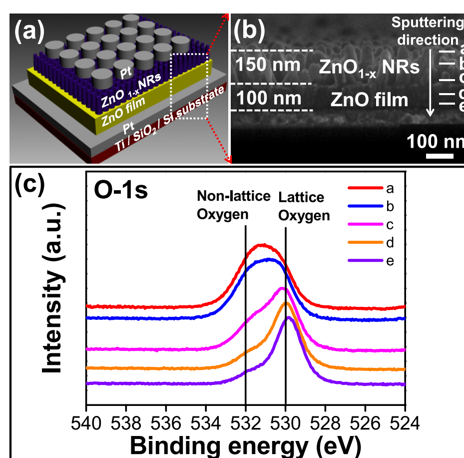

Figure 1. (a) Schematic of a Pt/ZnO_{1-x} NRs/ZnO TF/Pt resistive switching device. (b) Corresponding SEM image of a well-aligned ZnO_{1-x} NR with a length of ~150 nm grown on the ZnO film with a thickness of ~100 nm. (c) XPS at the O 1s-edge spectra related to different regions labeled from a to e in (b).

~30.7 A/cm^2 at −2 V could be obtained, yielding a rectifying ratio of ~160 at ±2 V. In addition, the rectifying characteristic of the ZnO_{1-x} NRs/ZnO TF structure device is very stable even through the device was opertated for over 1000 cycles as shown in Figure S2a. However, a rather larger ideality factor of 11.9 extracted from a logarithmic plot of the $I-V$ curve as shown in Figure S2b is due to the larger series resistances resulting from the ZnO TF and the ZnO_{1-x} NRs.[24] Furthermore, by applying a dc voltage of ~3.4 V with a compliance current of ~10 mA, namely, the "forming process", we are able to tune the devices from the diode to the resistive switching memory, for which an abrupt increasing of current was observed owing to formation of conducting filaments located inside the ZnO TF device, leading to a device in a low-resistance state (LRS), as shown in Figure 2b. The higher initial resistive state of the ZnO_{1-x} NRs/ZnO TF bilayer structure needs a larger forming voltage to trigger the migration of oxygen vacancies from the ZnO_{1-x} NRs to the ZnO TF layer compared to only a ZnO TF device with the less forming voltage of ~2.8 V. Once a negative bias of ~−0.7 V was applied, the ZnO_{1-x} NRs/ZnO TF bilayer device changes to a high-resistance state (HRS), which is called a "RESET" process. Furthermore, a change of resistance from HRS to LRS, namely, a "SET" process, could be achieved after an applied positive voltage of 1.3 V, as shown in Figure 2c.[3−5] The reduction of the SET voltage for the ZnO_{1-x} NRs/ZnO TF bilayer device compared to the TF could be distinctly observed, which is most likely due to the diffusion of oxygen vacancies confined by the ZnO_{1-x} NRs into the ZnO TF for the recovery of conducting filaments. Moreover, the threshold voltages for the switching in terms of the cumulative distribution of the V_{SET} and V_{RESET} and resistances of

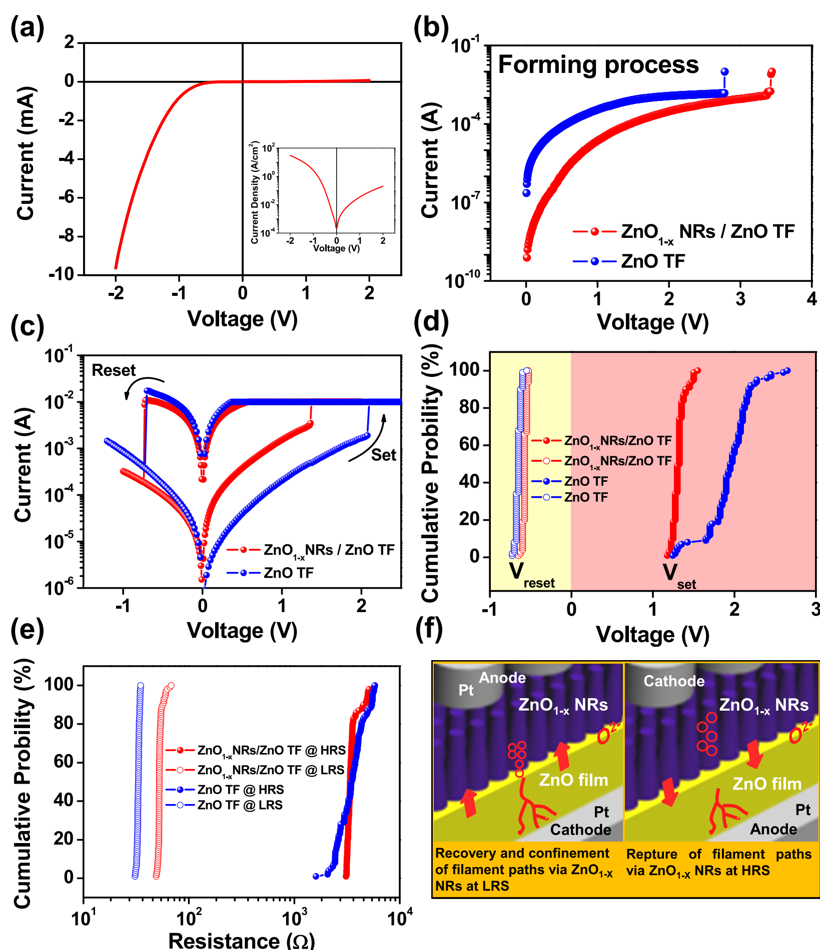

Figure 2. (a) $I-V$ curve of Pt/ZnO_{1-x} NRs/ZnO TF/Pt diode device. Inset shows the corresponding current density−voltage ($J-V$) curve. (b) $I-V$ curves of forming process for the Pt/ZnO_{1-x}NRs/ZnO TF/Pt and the Pt/ZnO TF/Pt devices. (c) Bipolar $I-V$ characteristics for the Pt/ZnO_{1-x} NRs/ZnO TF/Pt and the Pt/ZnO TF/Pt devices. Cumulative distribution of (d) the SET/RESET voltages and (e) resistances of HRS/LRS for the Pt/ZnO_{1-x} NRs/ZnO TF/Pt and the Pt/ZnO TF/Pt devices. (f) Confined recovery and rupture of conducting filaments by ZnO_{1-x} NRs.

the HRS and LRS at a read voltage of 0.1 V for both the ZnO_{1-x} NRs/ZnO TF bilayer and ZnO TF devices were measured as shown in Figure 2d and e, respectively. Obviously, a very narrow distribution of the SET voltage of 1.2−1.5 V and a uniform ratio of R_{HRS}/R_{LRS} could be observed. The corresponding endurance tests of ∼100 cycles at the V_{SET} and V_{RESET} voltages and resistances of the HRS and LRS with a read voltage of 0.1 V are shown in Figure S3a and b, respectively. In general, the microstructure of materials would influence the diffusion of defects and vacancies in the device.[25,26] It is believed that oxygen vacancies prefer to migrate along preferred grain boundaries along [0001] to form the conducting filaments, for which the ZnO_{1-x} NRs play an important role as a supplementary reservoir of oxygen vacancies to confine the recovery and rupture of conducting filaments, substantially resulting in improvement of device performance for the ZnO_{1-x} NRs/ZnO TF bilayer structure compared with that of the ZnO TF structure. The possible migration of oxygen vacancies from the ZnO_{1-x} NRs to the ZnO TF is schematically illustrated in Figure 2f. Once the SET voltage was applied, oxygen vacancies were repelled out of the ZnO_{1-x} NRs into the ZnO TF layer to confine the recovery of conducting filaments, while the oxygen anions were further attracted from the ZnO_{1-x} NRs to compensate conducting filaments after the RESET voltage was applied. On the other hand, the ZnO_{1-x} NRs/ZnO TF device could also be stably operated with a unipolar resistive switching behavior, as shown in Figure S4a, for which the switching behavior does not depend on the bias polarity.[3,4] Switching the device from HRS to LRS by an applied voltage of ∼1.5 V is called a "SET" process, while converting the device into the HRS after the voltage was reapplied over ∼0.6 V is called a "RESET" process. Obviously, the SET voltage of the ZnO_{1-x} NRs/ZnO TF device decreases to ∼1.5 V compared with that of the ZnO TF device (V_{SET} = ∼1.8 V). The reduced SET voltage of the ZnO_{1-x} NRs/ZnO TF device operating in the unipolar mode is most likely due to the supplement of oxygen vacancies from the ZnO_{1-x} NRs to the ZnO TF for the recovery/rupture of metallic paths inside the ZnO. The endurance test of 100 cycles for the ZnO_{1-x} NRs/ZnO TF device under unipolar operation further

provides evidence of a stable performance, as shown in Figure S4b. In addition, the retention test of the ZnO_{1-x} NRs/ZnO TF devices was conducted to shed light on the reliability, with which resistances of ~50 and ~2000 Ω at LRS and HRS with a read voltage of 0.1 V could be achieved, yielding a very stable R_{HRS}/R_{LRS} ratio of 40 (Figure S5a). No degradation at $>10^4$ s for the ZnO_{1-x} NRs/ZnO TF device indicates a good retention performance, which is compatible with that of the ZnO TF device (Figure S5b).

To understand the resistive switching characteristics, the classical nonlinear conduction mechanisms, including Schottky-like emission,[27] Poole–Frenkel (PF) emission,[28] and space charge limited current,[29] were adopted to fit the nonlinearity of the measured J–E curves, for which PF emission is given as[28]

$$J \propto E \exp\left(\frac{\sqrt{q^3 E/\pi \varepsilon_r \varepsilon_0}}{r k_B T}\right)$$

where q is the electrical charge, ε_r is the dynamic dielectric constant, ε_0 is the vacuum permittivity, k_B is the Boltzmann constant, T is the temperature, and r is a coefficient ranging between 1 and 2. A normal PF emission happens at $r = 1$, indicating carriers hopping *via* trapped states excited by an electrical field, while large amounts of defects formed in the junction could eventually result in a modified PF emission, namely, a Schottky-like emission at $r = 1-2$.[30] By fitting the $\ln(J/E)$ as a function of the square root of E at the HRS, as shown in Figure 3a, an ohmic conduction for both devices was observed in the low-voltage region and turns into a nonlinear behavior in the high-voltage region (Figure S6). The slopes of 14.9 and 11.0 with a refractive index of ~2 could be found to perfectly match the fitting of PF emission, yielding $r = 1$ and $r = 1.4$ for the Pt/ZnO TF/Pt and the Pt/ZnO_{1-x} NRs/ZnO TF/Pt devices, respectively.[30] The results indicate that normal PF emission occurred in the ZnO TF at HRS. However, the modified PF emission, namely, the Schottky-like emission, dominates the transport mechanism for the ZnO_{1-x} NRs/ZnO bilayer structure at the HRS, resulting in asymmetric I–V behavior because of the asymmetric Schottky barrier heights (Figure 2c).[31,32] In the HRS, the resistance is mainly determined by the ZnO TF, which has a relatively higher resistance than that of the ZnO_{1-x} NRs, thereby no obvious resistance difference at the HRS for both the ZnO_{1-x} NRs/ZnO TF bilayer and ZnO TF devices, respectively (Figure 2e). However, after tuning both devices into the LRS, the resistance is mainly limited by the ZnO_{1-x} NRs because of the relatively higher resistance compared to ZnO TF since the ZnO TF exhibits a metallic behavior due to the formation of conducting filaments. To further shed light on the scaling issue, the currents of the LRS and HRS at different electrode sizes at a read voltage of 0.1 V for both types of devices were measured as shown in Figure 3b. The current in the HRS for both devices

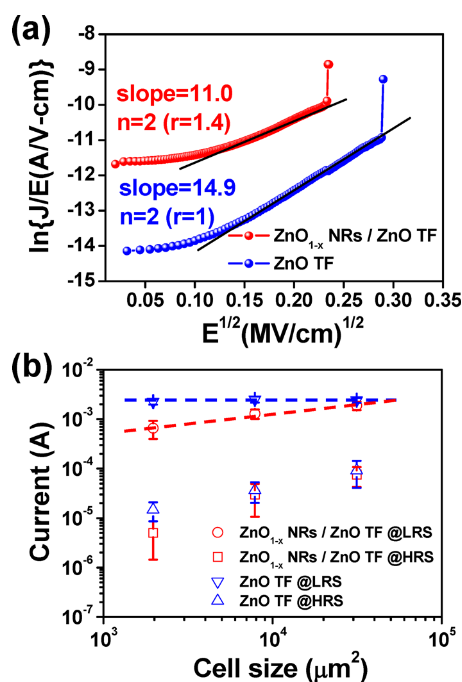

Figure 3. (a) $\ln(J/E)$–$E^{1/2}$ plots for the Pt/ZnO_{1-x} NRs/ZnO TF/Pt and the Pt/ZnO TF/Pt devices. (b) Currents as a function of measured electrode sizes at HRS/LRS for the Pt/ZnO_{1-x} NRs/ZnO TF/Pt and the Pt/ZnO TF/Pt devices. The error bar at each electrode size is calculated by the standard deviation of 20 devices.

decreases as the electrode size decreases. In the LRS, the current of the Pt/ZnO TF/Pt devices is independent of the electrode size owing to the metallic feature resulting from the formation of local conducting filaments in the ZnO TF, while the current of Pt/ZnO_{1-x} NRs/ZnO TF/Pt devices decreases as the measured electrode sizes were decreased, namely, an inversely linear dependence. The results indicate that the total current in the LRS is limited by the relatively high resistance of the ZnO_{1-x} NRs layer. Therefore, the use of the ZnO_{1-x} NRs grown on ZnO TF not only presents as a reservoir which provides oxygen vacancies but also acts as a buffer layer to prevent failure of devices from a high current flux as the dimension of the device is decreased. In addition, the length of ZnO NWs also affects the resistivity of the whole bilayer device. Notably, the resistivity of the NRs layer must be controlled to within a certain resistivity window compared with that of ZnO TF. If the resistivity of the ZnO NR layer is too high, the voltage drop across the NR layer would not be negligible, compared with that of ZnO TF, and the forming process would occur across the entire device, namely, ZnO NRs + ZnO TF. On the other hand, if the resistivity of the ZnO NR layer is too low, the NR layer acts only as a simple metallic contact.[21]

The adsorption of water molecules or metallic dust nanoparticles on the surface of a device in a real environment may easily result in a short circuit or a malfunction during operation of a ReRAM device. Therefore, a suitable package of an entire device is a conventional method of preventing the damage of a

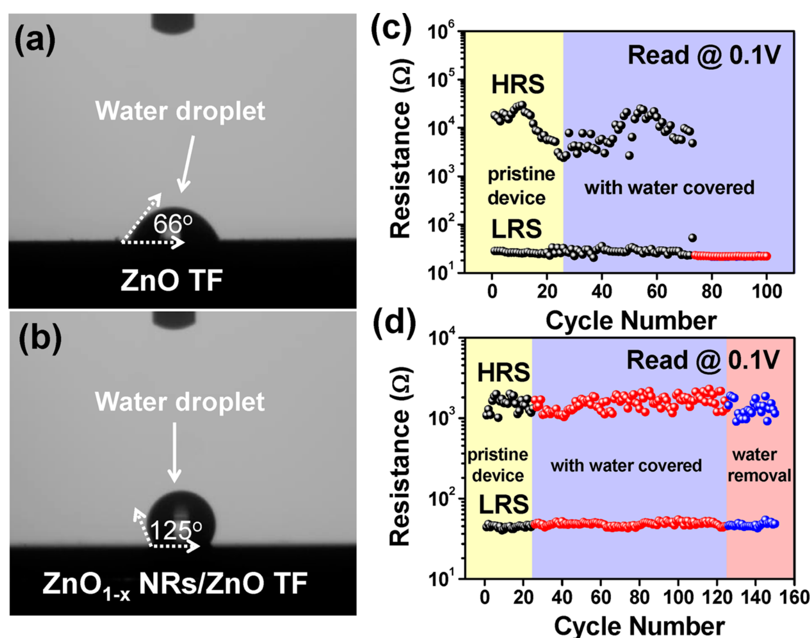

Figure 4. (a, b) Contact angle measurements for surfaces of the ZnO film and the ZnO_{1-x} NRs, respectively. (c, d) Corresponding endurance tests for two devices measured with coverage of a water droplet at a read bias of 0.1 V, respectively.

device when contacting water. Alternatively, the surface self-cleaning function due to a hydrophobic behavior could be considered as another good approach to split the water from the device surface. Contact angle (CA) measurement is a typical method to determine the surface hydrophobicity or hydrophilicity.[33] Figure 4a and b show the optical images of contact angle measurements at devices without and with the growth of the ZnO_{1-x} NRs. The contact angle of ~66° could be obtained for the ZnO TF device, indicating a slight hydrophilicity, while the contact angle increases to ~125°, indicating a hydrophobicity after the growth of the ZnO_{1-x} NRs on the ZnO TF without any surface modification. The hydrophobic surface could be simply expressed by a Cassie model in terms of surface fraction of the solid and air pocket:[34]

$$\cos\alpha = f_1 \cos\beta - f_2$$

where α is the apparent contact angle, f_1 is the surface fraction of the solid, f_2 is the surface fraction of air pocket, and β is the contact angle on a flat surface. The small surface fraction of the solid owing to the formation of the ZnO_{1-x} NRs leads to the increase of the larger surface fraction of the air pocket inside the ZnO_{1-x} NRs, eventually resulting in a larger CA to prevent the penetration of water molecules into the device. In addition, by increasing the aspect ratio *via* growing longer ZnO_{1-x} NRs, we are able to further increase the CA to >150°, which agrees with a report in the literature.[35−37] To evaluate the surface self-cleaning function, the endurance tests at a read bias of 0.1 V for both devices without and with coverage of a water droplet were measured as shown in Figure 4c and d (see Supporting Information for the detailed measurements). Consequently, the endurance test of the ZnO TF device was unstable, eventually resulting in a short circuit after ~50 cycles (68th cycle). However, the ZnO_{1-x} NRs/ZnO TF device has a very stable endurance over 100 cycles during the coverage of the water droplet and is still intact after removal of the water droplet at the 125th cycle.

Finally, we are able to combine the ZnO_{1-x} NRs/ZnO TF homojunction diode and the ZnO_{1-x} NRs/ZnO TF resistive memory into a complementary 1D1R resistive switching device, namely, a Pt/ZnO_{1-x} NRs/ZnO TF/Pt/ZnO TF/ZnO_{1-x} NRs/Pt stacking structure, by simply connecting two identical devices back to back in series in order to simplify the fabrication process. Figure 5a shows the corresponding *I*−*V* characteristics of the complementary 1D1R structure. The inset shows the stacking sequence of two devices and a representative equivalent circuit with representative symbols of the memristor and the diode, respectively. Note that the complementary 1D1R also required an initial forming process to switch one of the devices into the unipolar resistive switching (memory device) with a positive voltage of ~5.8 V. Obviously, the resistance switching at SET and RESET voltages could be achieved after a forward bias of ~3.2 and ~1.8 V, respectively, while at a reverse bias, the diode could suppress the current. (More devices are shown in Figure S9.) Comparing the SET and RESET voltages of a 1R device with that of the complementary 1D1R device, the increasing of SET and RESET voltages could be explained due to increasing of the total resistance by the memory cell in series with the diode. In addition, the stable endurance test of ~90 cycles and the retention test up to 10^4 s at a high read bias of 1 V as shown in Figure 5b

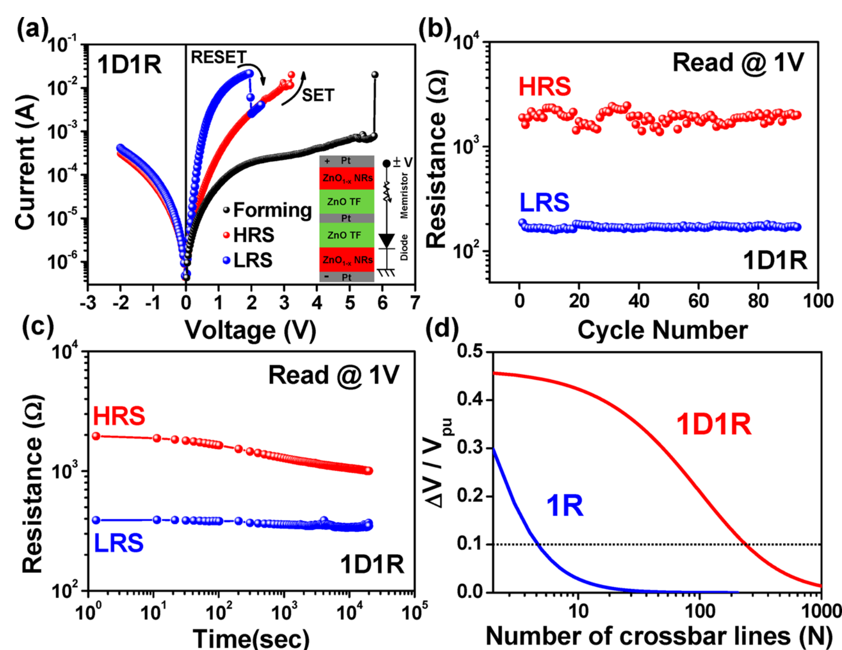

Figure 5. (a) $I-V$ characteristics of the complementary 1D1R devices with which the Pt/ZnO_{1-x} NRs/ZnO TF/Pt and Pt/ZnO TF/ZnO_{1-x} NRs/Pt act as the memory cell and diode, respectively. Inset shows a schematic of the device configuration and the corresponding equivalent circuit with representative symbols of the diode and resistor. Corresponding resistance at the HRS and LRS at a high read voltage of 1 V for (b) the endurance test of 90 cycles and (c) the retention test. (d) Dependence of $\Delta V/V_{pu}$ on the crossbar line number (N) at read voltages of 0.1 and 0.7 V for the 1R cells and the completer 1D1R devices.

and c, respectively, reveal that the complementary 1D1R has a reliable performance. To estimate the maximum array density of the complementary 1D1R, two passive crossbar arrays (N rows $\times$ N columns) using the memory cells (1R) and the complementary 1D1R devices with a measurably normalized read voltage margin, $\Delta V/V_{pu}$, at 0.1 and 0.7 V for the 1R and the complementary 1D1R as an important parameter of estimating the cross array density are shown in Figure 5d (for a more detailed calculation, see the Supporting Information). Notably, the read margin decreases as the crossbar number (N) increases for both the 1R cells and the complementary 1D1R devices. Therefore, the maximum N numbers of 3 and 240 for the 1R cells and the complementary 1D1R devices could be achieved by taking a $\Delta V/V_{pu}$ of 0.1 (10%) into account, respectively. The results demonstrate a promising application of a ZnO_{1-x} NRs/ZnO TF bilayer structure as a complementary 1D1R device for 3D crossbar arrays and also provide an opportunity for an all-ZnO-based memory system in a low-temperature process. Further, by increasing the ON/OFF ratio of the ZnO_{1-x} NRs/ZnO TF bilayer structure diode *via* decreasing the ideality factor through process optimization and electrode/ZnO interface engineering, the ratio of R_{sneak}/R_{LRS} is expected to increase, thereby further enlarging the crossbar array numbers.

CONCLUSIONS

We presented the growth of ZnO_{1-x} nanorod arrays on a ZnO thin film as homojunction diode and memory devices, containing uniquely double behaviors, namely, rectifying and high-performance resistive switching behaviors, depending on the applied voltages, simultaneously. The ZnO_{1-x} NRs act as the reservoir for supplemental oxygen vacancies to reduce the operation voltage, thereby significantly improving the ReRAM device performance. In addition, by utilizing the ZnO_{1-x} NR surface, a contact angle of ~125° can be found, demonstrating the self-cleaning effect due to a hydrophobic behavior. The all-ZnO-based memory system with the complementary 1D1R structure for possible application in passive crossbar arrays was successfully demonstrated. Our work provides a novel concept to enhance memory performance by adding one-dimensional ZnO_{1-x} NRs in a low-temperature process, realizing the potential of an all-ZnO-based memory system.

METHODS

Device Fabrications. A 100-nm-thick ZnO thin film was deposited on a Pt/Ti/SiO_2/Si substrate at room temperature by radio frequency magnetron sputtering using a ZnO target in an Ar atmosphere. ZnO_{1-x} NRs were grown using a chemical bath deposition method. The ZnO film substrate as a seed layer was placed in an aqueous solution (100 mL) mixed with zinc nitrate hexahydrate (0.02 M, $Zn(NO_3)_2 \cdot 6H_2O$, 98%, Aldrich) and hexamethylenetetramine (0.02 M, $C_6H_{12}N_4$, HMTA, 99.5%, Riedel-de Haen). The substrate was upside down inside the solution.

The solution and substrate were placed at 95 °C in a heated oven for 0.5 h for the NR growth. After the NR growth, the substrate was rinsed with deionized water and baked at 80 °C. The Pt as the top electrode with a thickness of 100 nm was deposited on the ZnO_{1-x} NRs *via* rf-magnetron sputtering at room temperature. The Pt electrodes of diameters 200, 100, and 50 μm were fabricated *via* a metal shadow mask.

Characterizations. The electrical characterizations and resistive switching characteristics of the fabricated devices were investigated using a Keithley 4200 semiconductor parameter analyzer in voltage sweeping mode at room temperature. All of the operation voltages were applied on the top Pt electrode, and the Pt bottom electrode was grounded. The surface morphology of the ZnO_{1-x} NRs was examined by field-emission scanning electron microscopy (JSM-6500F, JEOL). The chemical bonding states were characterized by X-ray photoelectron spectroscopy (PHI 1600). The contact angles were measured using 5 μL droplets of deionized water under an ambient atmospheric condition.

Conflict of Interest: The authors declare no competing financial interest.

Acknowledgment. This research was supported by the National Science Council through grant nos. NSC 101-2112-M-007-015-MY3 and NSC-100-2120-M-007-008 and National Tsing Hua University through grant no. 100N2024E1. The authors C.H.H., J.-S.H., S.M.L., and Y.L.C. greatly appreciate the use of the facility at CNMM at the National Tsing Hua University through grant no. 101N2744E1.

Supporting Information Available: Detailed experimental section for device fabrication and characterization; $I-V$ curve of a Pt/ZnO TF/Pt device; endurance characteristics of the Pt/ZnO_{1-x} NRs/ZnO TF/Pt diode and linear fitting of the Pt/ZnO_{1-x} NRs/ZnO TF/Pt diode; endurance test at HRS/LRS and SET/RESET voltages with 100 cycles for the Pt/ZnO_{1-x} NRs/ZnO TF/Pt device and the Pt/ZnO TF/Pt device; retention test for the Pt/ZnO_{1-x} NRs/ZnO TF/Pt device and the Pt/ZnO TF/Pt device; $I-V$ curves and endurance test for the Pt/ZnO_{1-x} NRs/ZnO TF/Pt resistive memory device at a unipolar operation; conducting mechanism with an ohmic behavior in the low-voltage region; detailed processes of measurement when the device is covered by water droplets; optical images of both devices measured under the coverage of water droplets; more $I-V$ curves of the complementary 1D1R devices; calculation of maximum crossbar lines in a read margin for the Pt/ZnO_{1-x} NRs/ZnO TF/Pt resistor cell and the complementary 1D1R device. These materials are available free of charge *via* the Internet at http://pubs.acs.org.

REFERENCES AND NOTES

1. Parkin, S. S. P.; Hayashi, M.; Thomas, L. Magnetic Domain-Wall Racetrack Memory. *Science* **2008**, *320*, 190–194.
2. Wuttig, M.; Yamada, N. Phase-Change Materials for Rewriteable Data Storage. *Nat. Mater.* **2007**, *6*, 824–832.
3. Waser, R.; Aono, M. Nanoionics-Based Resistive Switching Memories. *Nat. Mater.* **2007**, *6*, 833–840.
4. Sawa, A. Resistive Switching in Transition Metal Oxides. *Mater. Today* **2008**, *11*, 28–36.
5. Waser, R.; Dittmann, R.; Staikov, G.; Szot, K. Redox-Based Resistive Switching Memories—Nanoionic Mechanisms, Prospects, and Challenges. *Adv. Mater.* **2009**, *21*, 2632–2663.
6. Park, C.; Jeon, S. H.; Chae, S. C.; Han, S.; Park, B. H.; Seo, S.; Kim, D.-W. Role of Structural Defects in the Unipolar Resistive Switching Characteristics of Pt/NiO/Pt Structures. *Appl. Phys. Lett.* **2008**, *93*, 042102–3.
7. Zhang, H.; Liu, L.; Gao, B.; Qiu, Y.; Liu, X.; Lu, J.; Han, R.; Kang, J.; Yu, B. Gd-Doping Effect on Performance of HfO_2 Based Resistive Switching Memory Devices Using Implantation Approach. *Appl. Phys. Lett.* **2011**, *98*, 042105–3.
8. Syu, Y.-E.; Chang, T.-C.; Tsai, T.-M.; Chang, G.-W.; Chang, K.-C.; Tai, Y.-H.; Tsai, M.-J.; Wang, Y.-L.; Sze, S. M. Silicon Introduced Effect on Resistive Switching Characteristics of WO_x Thin Films. *Appl. Phys. Lett.* **2012**, *100*, 022904–4.
9. Lee, M. S.; Choi, S.; An, C.-H.; Kim, H. Resistive Switching Characteristics of Solution-Deposited Gd, Dy, and Ce-Doped ZrO_2 Films. *Appl. Phys. Lett.* **2012**, *100*, 143504–4.
10. Zhang, H.; Gao, B.; Sun, B.; Chen, G.; Zeng, L.; Liu, L.; Liu, X.; Lu, J.; Han, R.; Kang, J.; *et al.* Ionic Doping Effect in ZrO_2 Resistive Switching Memory. *Appl. Phys. Lett.* **2010**, *96*, 123502–3.
11. Chang, W.-Y.; Huang, H.-W.; Wang, W.-T.; Hou, C.-H.; Chueh, Y.-L.; He, J.-H. High Uniformity of Resistive Switching Characteristics in a Cr/ZnO/Pt Device. *J. Electrochem. Soc.* **2012**, *159*, G29–G32.
12. Yoon, J.; Choi, H.; Lee, D.; Park, J. B.; Lee, J.; Seong, D. J.; Ju, Y.; Chang, M.; Jung, S.; Hwang, H. Excellent Switching Uniformity of Cu-Doped MoO_x/GdO_x Bilayer for Nonvolatile Memory Applications. *IEEE Electron Device Lett.* **2009**, *30*, 457.
13. Lee, J.; Bourim, E. M.; Lee, W.; Park, J.; Jo, M.; Jung, S.; Shin, J.; Hwang, H. Effect of ZrO_x/HfO_x Bilayer Structure on Switching Uniformity and Reliability in Nonvolatile Memory Applications. *Appl. Phys. Lett.* **2010**, *97*, 172105–3.
14. Chang, W.-Y.; Cheng, K.-J.; Tsai, J.-M.; Chen, H.-J.; Chen, F.; Tsai, M.-J.; Wu, T.-B. Improvement of Resistive Switching Characteristics in TiO_2 Thin Films with Embedded Pt Nanocrystals. *Appl. Phys. Lett.* **2009**, *95*, 042104–3.
15. Liu, Q.; Long, S.; Lv, H.; Wang, W.; Niu, J.; Huo, Z.; Chen, J.; Liu, M. Controllable Growth of Nanoscale Conductive Filaments in Solid-Electrolyte-Based ReRAM by Using a Metal Nanocrystal Covered Bottom Electrode. *ACS Nano* **2010**, *4*, 6162–6168.
16. Lee, W.; Park, J.; Kim, S.; Woo, J.; Shin, J.; Lee, D.; Cha, E.; Hwang, H. Improved Switching Uniformity in Resistive Random Access Memory Containing Metal-Doped Electrolyte due to Thermally Agglomerated Metallic Filaments. *Appl. Phys. Lett.* **2012**, *100*, 142106–4.
17. Kim, T.-W.; Choi, H.; Oh, S.-H.; Wang, G.; Kim, D.-Y.; Hwang, H.; Lee, T. One Transistor—One Resistor Devices for Polymer Non-Volatile Memory Applications. *Adv. Mater.* **2009**, *21*, 2497–2500.
18. Cho, B.; Kim, T.-W.; Song, S.; Ji, Y.; Jo, M.; Hwang, H.; Jung, G.-Y.; Lee, T. Rewritable Switching of One Diode—One Resistor Nonvolatile Organic Memory Devices. *Adv. Mater.* **2010**, *22*, 1228–1232.
19. Linn, E.; Rosezin, R.; Kugeler, C.; Waser, R. Complementary Resistive Switches for Passive Nanocrossbar Memories. *Nat. Mater.* **2010**, *9*, 403–406.
20. Lee, M.-J.; Lee, C. B.; Lee, D.; Lee, S. R.; Chang, M.; Hur, J. H.; Kim, Y.-B.; Kim, C.-J.; Seo, D. H.; Seo, S.; *et al.* A Fast, High-Endurance and Scalable Non-Volatile Memory Device Made from Asymmetric Ta_2O_{5-x}/TaO_{2-x} Bilayer Structures. *Nat. Mater.* **2011**, *10*, 625–630.
21. Yang, Y. C.; Pan, F.; Liu, Q.; Liu, M.; Zeng, F. Fully Room-Temperature-Fabricated Nonvolatile Resistive Memory for Ultrafast and High-Density Memory Application. *Nano Lett.* **2009**, *9*, 1636–1643.
22. Greene, L. E.; Yuhas, B. D.; Law, M.; Zitoun, D.; Yang, P. Solution-Grown Zinc Oxide Nanowires. *Inorg. Chem.* **2006**, *45*, 7535–7543.
23. Hsieh, P. T.; Chen, Y. C.; Kao, K. S.; Wang, C. M. Luminescence Mechanism of ZnO Thin Film Investigated by XPS Measurement. *Appl. Phys. A: Mater. Sci. Process.* **2008**, *90*, 317–321.
24. Cheung, S. K.; Cheung, N. W. Extraction of Schottky Diode Parameters from Forward Current-Voltage Characteristics. *Appl. Phy. Lett.* **1986**, *49*, 85–87.
25. Lee, M.-J.; Han, S.; Jeon, S. H.; Park, B. H.; Kang, B. S.; Ahn, S.-E.; Kim, K. H.; Lee, C. B.; Kim, C. J.; Yoo, I.-K.; *et al.* Electrical Manipulation of Nanofilaments in Transition-Metal Oxides for Resistance-Based Memory. *Nano Lett.* **2009**, *9*, 1476–1481.
26. Mo, X.-L.; Chen, G.-R.; Cai, Q.-J.; Fan, Z.-Y.; Xu, H.-H.; Yao, Y.; Yang, J.; Gu, H.-H.; Hua, Z.-Y. Preparation and Electrical/Optical Bistable Property of Potassium Tetracyanoquinodimethane Thin Films. *Thin Solid Films* **2003**, *436*, 259–263.
27. Emtage, P. R.; Tantraporn, W. Schottky Emission Through Thin Insulating Films. *Phys. Rev. Lett.* **1962**, *8*, 267–268.

28. Yeargan, J. R.; Taylor, H. L. The Poole-Frenkel Effect with Compensation Present. *J. Appl. Phys.* **1968**, *39*, 5600–5604.
29. Lampert, M. A. Simplified Theory of Space-Charge-Limited Currents in an Insulator with Traps. *Phys. Rev. Lett.* **1956**, *103*, 1648–1656.
30. Chang, W.-Y.; Lai, Y.-C.; Wu, T.-B.; Wang, S.-F.; Chen, F.; Tsai, M.-J. Unipolar Resistive Switching Characteristics of ZnO Thin Films for Nonvolatile Memory Applications. *Appl. Phys. Lett.* **2008**, *92*, 022110–3.
31. Yang, J. J.; Pickett, M. D.; Li, X.; OhlbergDouglas, A. A.; Stewart, D. R.; Williams, R. S. Memristive Switching Mechanism for Metal/Oxide/Metal Nanodevices. *Nat. Nano.* **2008**, *3*, 429–433.
32. Yang, J. J.; Borghetti, J.; Murphy, D.; Stewart, D. R.; Williams, R. S. A Family of Electronically Reconfigurable Nanodevices. *Adv. Mater.* **2009**, *21*, 3754–3758.
33. Kwok, D. Y.; Neumann, A. W. Contact Angle Measurement and Contact Angle Interpretation. *Adv. Colloid Interface Sci.* **1999**, *81*, 167–249.
34. Cassie, A. B. D.; Baxter, S. Wettability of Porous Surfaces. *Trans. Faraday Soc.* **1944**, *40*, 546–551.
35. Hsieh, C. T.; Yang, S. Y.; Lin, J. Y. Electrochemical Deposition and Superhydrophobic Behavior of ZnO Nanorod Arrays. *Thin Solid Films* **2010**, *518*, 4884–4889.
36. He, G. P.; Wang, K. G. The Super Hydrophobicity of ZnO Nanorods Fabricated by Electrochemical Deposition Method. *Appl. Surf. Sci.* **2011**, *257*, 6590–6594.
37. Ko, H.; Zhang, Z.; Chueh, Y.-L.; Ho, J. C.; Lee, J.; Fearing, R. S.; Javey, A. Wet and Dry Adhesion Properties of Self-Selective Nanowire Connectors. *Adv. Funct. Mater.* **2009**, *19*, 3098–3102.